*Arab J. Nucl. Sci. Appl., Vol. 55, 4, 79-91 (2022)*

ISSN 1110-0451

**Arab Journal of Nuclear Sciences and Applications**

Web site: ajnsa.journals.ekb.eg

(E S N S A)

# Evaluation of Gamma Activity Concentrations ($^{226}Ra$, $^{232}Th$, $^{40}K$) AND Related Potential Radiological Risks in Granitic Rocks from Nuweibi Mining Area, Egyptian Nubian Shield

**Mohamed Th. S. Heikal [1], Waleed M. Abdellah [2], Mohamed Salem Kamar [3], Mohamed. O. Ibrahim [3*] and Mohamed Abd El Monsef [1]**

(1) *Geology Department, Faculty of Science, Tanta University, Egypt*

(2) *Radiation Protection Department, Nuclear and Radiological Safety Research Center, Egyptian Atomic Energy Authority, Cairo, Egypt*

(3) *Nuclear Materials Authority, El Qatamiya, Cairo, Egypt*

ARTICLE INFO

*Article history:*

Received: 18th Feb. 2022

Accepted: 14th June 2022

*Keywords:*

*Nuweibi;*
*albite granite;*
*Nubian Shield;*
*natural radioactivity;*
*HPGe spectroscopy;*
*radiation risk assessment.*

ABSTRACT

**In the present study, we focus on the activity concentrations of $^{226}Ra$, $^{232}Th$ and $^{40}K$ measured using HPGe in twenty-six (26) albite granite and granodiorite samples from the Nuweibi mining area in the central Eastern Desert between latitudes 25° 11\ 30\\ to 25° 12\ 35\\ N and longitudes 34° 28\ 50\\ to 34° 30\ 10\\ E, which is a part of the Egyptian Nubian Shield of Neoproterozoic age. The Nuweibi geology comprises an ophiolite assemblage (serpentinites and metagabbros), tuffaceous metasediments, syntectonic older granitoids (granodiorite and tonalite) and finally post-collisional younger granites (albite granite). The average activity concentrations were 11.2, 11.9 and 289 Bq/kg for $^{226}Ra$, $^{232}Th$ and $^{40}K$ in the granodiorite samples, and 42.2, 71.5 and 811 in the albite granites, respectively. Absorbed gamma dose rates (ADRA) were 24.50 nGy/h for granodiorites and 97.72 nGy/h for albite granites, and outdoor annual effective doses ($AED_{out}$) were 0.03 mSv/year for granodiorites, and 0.12mSv/year for albite granites, respectively. Calculated gamma absorbed dose rates in air and annual outdoor effective doses were also compared with literature in terms of health issues and environmental impacts of workable albite granite in the area of study.**

## INTRODUCTION

Almost granite and rhyolite rocks (felsic igneous rocks) saturated with $SiO_2$, contain higher amounts of natural radionuclides than other rock types [1-5]. The amount of radionuclides in them differs depending on their mineral composition and origin. Several studies have been conducted to take into account the natural radioactivity levels and radiological risk parameters in granitic rocks from the Egyptian Nubian Shield both in the Eastern Desert and the southern Sinai Peninsula [6-8]. The activity concentrations of $^{226}Ra$, $^{232}Th$ and $^{40}K$ in the granitic rocks collected from the Neuwibi mining area are reported in the present study. Primitive publications referring to the present area, concern the radioactivity levels of these granites [9].

The Nuweibi mining area (~7 km$^2$) is located about 50 km northwest of Marsa Alam town (Fig.1). The area is characterized by the enrichment of albite-granite-hosted and quartz veins rare metals and cassiterite giving rise to the promising mining and quarrying area [10-12].

Regarding the study area, the main rock units constitute albite granite, granodiorite-tonalite and ophiolitic mélange (Fig.1). They are mainly sheared by strike-slip fault trending N-S and shear zones trending E-W and NE-SW and dissected by a series of mafic and felsic dykes (basalt to aplite) in addition to quartz and amazonite-rich veins.

The main purpose of this study is to evaluate the activity concentrations of natural radionuclides ($^{226}Ra$, $^{232}Th$, $^{40}K$) in the granitic rocks collected from the Nuweibi mine site area (Table 1) and thereby to provide data to literature from this area that have not been investigated in terms of radioactivity in details before. Thus, the reference scheme [2,3] for the radioactivity level of rare metal granite in the Egyptian Nubian Shield will be derived. In addition, whether it poses a potential radiological hazard in terms of public health and mine workers' health will be evaluated as well.

## GEOLOGY AND PETROGRAPHIC SIGNATURE

The present study of the Nuweibi albite granite (NAG) area lies between lat. 25° 12′ to 25° 12′ 30″ N and long. 34° 29″ to 34° 29′ 35″ E, covering an area about 7 km$^2$ (Fig.1). In the past, the area has attracted

Corresponding author: drmohamedosama92@gmail.com
DOI: 10.21608/ajnsa.2022.122489.1553

many investigators [10-12] due to the enrichment of tantalite-columbite and cassiterite (Ta-Nb-Sn) mineralization that assign the Nuweibi albite granite as a promising mining area both in the present and in the future particularly for these significant strategic minerals needed for versatile modern industries such as electronics and others.

The Nuweibi geology Comprises an ophiolite assemblage (serpentinites and metagabbros), tuffaceous metasediments, syntectonic older granitoids (granodirite andtonalite) and a single phase of post-collisional younger granite represented by albite granite (Fig.1). The studied granites (~4.5 km$^2$) represent the main focus of the investigation is divided into eastern and western parts by a strike-slip fault (N-S) along which the Wadi Nuweibi runs (Fig. 1). The granites in the eastern part intrude the tuffaceous metasediments giving rise to a narrow strip of hornfelses as well as granodiorite-tonalite. The albite granites in the western part are surrounded mostly by granodiorite-tonalite. Granitic apophyses and aplite-basaltic dikes traverse/dissect almost country rocks. Several shear zones occur within albite granites, in particular, the western part, trending E-W, NE-SW and N-S (Figs.1 and 2a). Recently, Emam et al. (2018)[11] calculated U–Pb columbite age in the albite granite of Nuweibi area (~ 620 Ma).

To determine the radioactivity levels of the studied granitic rocks, several ground gamma measurements are performed using RS-230 BGO Super-Spec. A portable detector has been used for the ground gamma measurements of surface outcrops of massive and sheared the Nuweibi albite granite (Fig. 2 b-c) and granodiorite-tonalite rocks. The ground gamma data range from 4.1 to 5.4 % (K%), 5.4 to 13.4 ppm (eU) and 27.4 to 58 ppm (eTh) referring to the albite granite, whereas the same concentrations of granodiorite-tonalite were including K% (1.5-2.4%), eU (2.3-28 ppm) and eTh (5.5-7.2 ppm).

Petrographically, the albite granite consists of sodic plagioclase, primary and secondary albite (An $_{5-12}$) giving rise to snowball textures, in particular the eastern part of the stock (Fig.3a) and potash feldspar including microcline together with quartz. Few accessory minerals represented by zircon, apatite (Fig.3a) and fluorite as well as tantalite-columbite are also present.

Granodiorite-tonalite consists of plagioclase (An $_{12-25}$), quartz with subordinate microcline and biotite (Fig.3b). Accessories include sphene, zircon and opaques. Hypidiomorphic texture is well survived (Fig.3b).

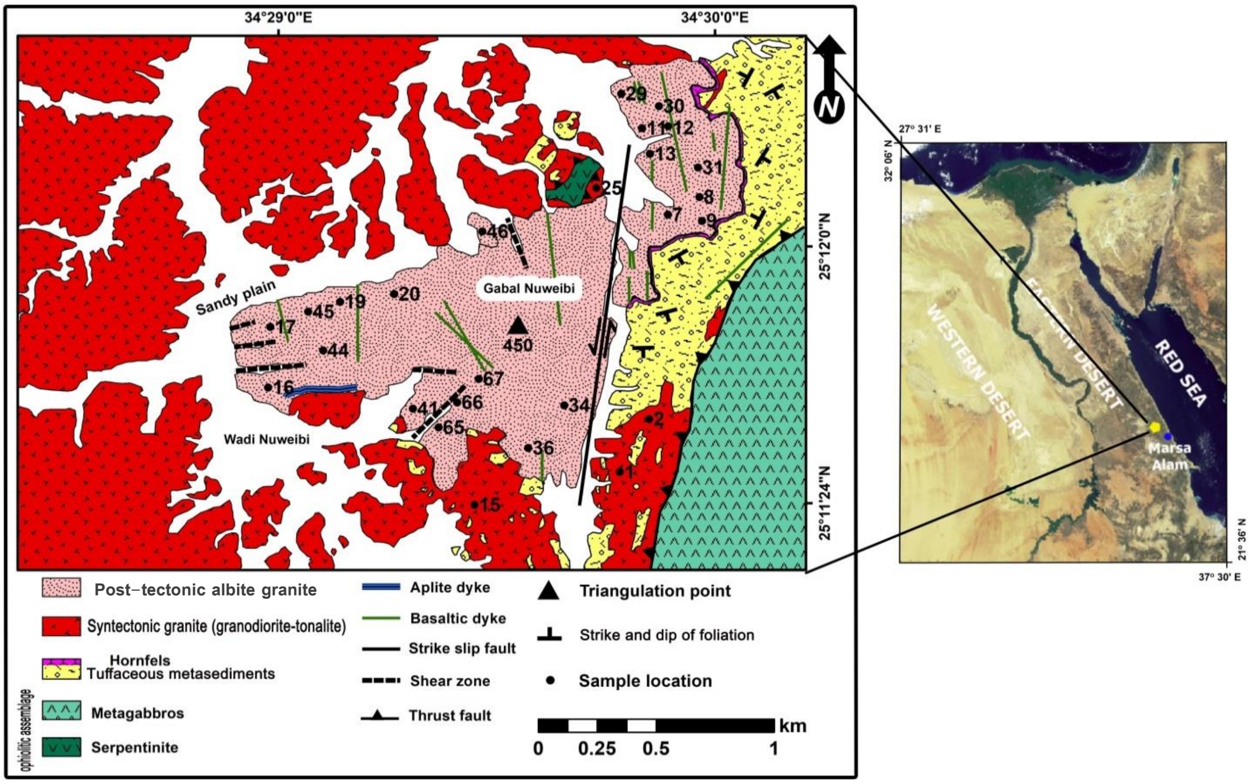


**Fig. (1) :** Geologic map of the Gabal Nuweibi area (modified after Helba et al, 1997[10] , Emam et al., 2018[11] and Azer et al., 2019[12]). The inset map indicates the location area. Sample locations refer to the samples collected for the gamma analyses using HPGe.


**Fig. 2a-c:** **a)** Master shear zone trending NE in albite granite. **b)** Ground gamma measurements of massive albite granite, using RS-230. **c)** Ground gamma measurements of highly sheared albite granite using RS-230.

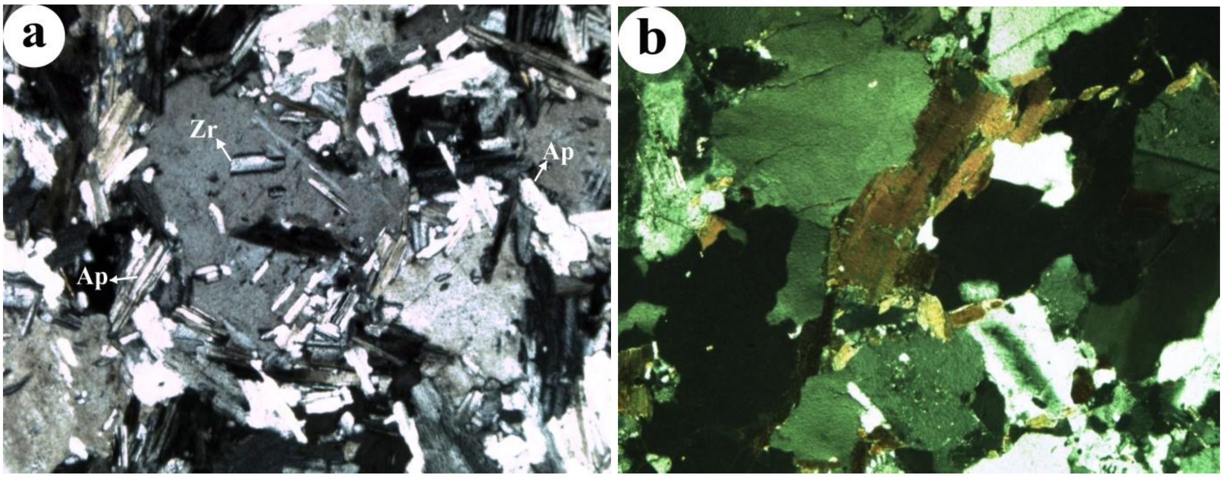


**Fig. 3a-b:** **a)** Snowball texture in albite granite Note zircon (Zr) and apatite (Ap) as inclusions within large crystal of quartz. Crossed polars, X40. **b)** Plagioclase, quartz and minor microcline and biotite giving rise to hypidiomorphic texture, granodiorite, crossed polars, X40.

## MATERIALS AND METHODS

### Sampling and sample preparation techniques and experimental setup

The samples were collected in two stages: A general radiation survey using a survey meter and after that systematic ground sampling [1,2]. The samples were marked at each sampling location (Fig.1a), using a GPS (Global Positioning System) device. After removing some alteration surfaces, 200 grams of rock samples were collected. The samples were packed in polyethylene bags, systematically labelled, and the coordinates of the sample locations were recorded using a GPS device. The samples were homogenized using an agate mortar at the sample preparation laboratory of the Department of Geology in the Tanta University (Egypt) and kept under normal conditions in the laboratory environment. All samples were kept tightly closed with gas-tight parafilm and stored for about 30 days in order to form a radioactive equilibrium between $^{226}$Ra and $^{222}$Rn. The selected samples were pulverized to a fine powder then, sieved through a 1 mm mesh size to remove the larger grains size and homogenized. Then, the samples were dried at a temperature-controlled furnace (oven) at 110 $^{o}$C for 24 hours to ensure that complete removal of moisture. After moisture removal, the samples were cooled down to room temperature in a desiccator.

At the same time, an empty container with the same geometry (Marinelli beakers of 100 cm$^3$ volume) used for samples was also sealed and left for a similar time with the samples in order to measure the background. The samples were then taken for gamma spectrometric analysis at the Radiation Protection Department in the Nuclear and Radiological Safety Research Center, Egyptian Atomic Energy Authority.

### Sample counting and detector efficiency calibration

The samples were placed into the active volume of a shielded high purity germanium (HPGe) detector with two inner concentric cylinders of lead, copper and cadmium, as well as its electronic circuits. A vertical Canberra N-type closed end-coaxial Canberra N-type HPGe detector (model GR4020) with about 40% relative efficiency and 2.0 keV energy resolution at 1.33 MeV photons of $^{60}$Co was used. This detector is shielded by a detector lead shield model 747/747E with Outer Jacket: 9.5 mm (3/8 in.) thick low carbon steel, Bulk Shield: 10 cm (4 in.) thick low background and Graded Lining: 1 mm (0.040 in.) tin and 1.6 mm (0.062 in.) copper. The spectra were analyzed using CANBERRA (Genie 2000) program [13].

The efficiency calibration of the analyzer channels using standard point sources is a procedure performed on a regular basis for the HPGe detector, as reported in the Genie-2000 Spectroscopy Software manual [13], which establishes a relationship between the energy of the gamma radiation and the number of channels. After the identification of the energy using standard sources, the detector was calibrated in absolute efficiency using mixed gamma sources with different radionuclides in the same geometry. The efficiency value is calculated by taking the probability of disintegration for each energy into account. This data is needed for efficiency calibration of the detector, as described in equation 1[14].

$$\varepsilon(E_\gamma) = \frac{NP \times M}{t_c \times I_\gamma(E_\gamma) \times A_{Ei}} \qquad \textbf{(1)}$$

Where: $\varepsilon(E_\gamma)$ is the detection efficiency at energy E, NP number of counts under the peak for the considered energy corrected for background, The activity concentration (in Bq/kg), $A_{Ei}$ of nuclide I and for peak at energy E, t is the counting time in sec, $I_\gamma(E_\gamma)$ the probability of gamma emission of the nuclide for a transition at energy E and M the mass in kg of the measured sample.

Quality Assurance was carried out by analysis of IAEA-381 [15] and IAEA Soil-6 [16] reference materials with a known concentration of natural radioactivity.

For the measurements of activity concentration (in Bq/kg), $A_{Ei}$ of nuclide i, each sample was counted for 72000 seconds (time) and spectra were analyzed using Genie 2000 software provides by Canberra Version V.3.2, including peak search, nuclide identification, activity and uncertainty calculation, and MDA calculation modules software based on the equation 2 [17].

$$A_{Ei}\left(\frac{Bq}{kg}\right) = \frac{NP}{t_c \times I_\gamma(E_\gamma) \times \varepsilon(E_\gamma) \times M} \qquad \textbf{(2)}$$

In the uranium series, the decay chain segment starting from radium ($^{226}$Ra) is radiologically the most important and, therefore, most of references are often used $^{226}Ra$ from its daughters as explained in our manuscript in addition to many references [18-22]. So, we focus in the decipated data on $^{226}Ra$ not in $^{238}U$ that results from 1001 keV because it has a lower probability 0.83% ratio and not accurate in measurements.

Under the assumption that secular equilibrium was reached between $^{232}Th$ and $^{238}U$ and their decay products, the γ-ray transitions to measure the concentration of the assigned nuclides in the series [14] are as follows:

- $^{234m}Pa$ (1001.03 keV) for $^{238}U$.
- $^{214}Bi$ (609.31, 1120.3 and 1764.49 keV), $^{214}Pb$ (295.22 and 351.93 keV) for $^{226}Ra$.
- $^{208}Tl$ (583.19 and 2614.53 keV), $^{212}Pb$ (238.63 and 300.09 keV) and $^{212}Bi$ (727.3 keV) for the $^{232}Th$ series.
- $^{228}Ac$ (338.32, 463.1, 911.20 and 968.97 keV) for $^{228}Ra$ and,
- (1460.83 keV) for $^{40}K$.

Statistical error calculation for measurement process [23,24], to correct the activity to actual activity in sample, we apply the necessary corrections to the count rate. Some typical corrections include: Counter efficiency, emission probability of emitted radiation, NP is net peak and the mass. The error in the activity is calculated with the propagation error Eq. (3).

$$\Delta A_{Ei} = A_{Ei} \times \sqrt{\left(\frac{\Delta M}{M}\right)^2 + \left(\frac{\Delta NP}{NP}\right)^2 + \left(\frac{\Delta I_\gamma(E_\gamma)}{I_\gamma(E_\gamma)}\right)^2 + \left(\frac{\Delta t_c}{t_c}\right)^2 + \left(\frac{\Delta\varepsilon(E_\gamma)}{\varepsilon(E_\gamma)}\right)^2} \quad \textbf{(3)}$$

**Statistical analysis**

STATGRAPHICS Centurion XVI statistical programme is used for summary analyses and for box and whisker depiction groups.

**Gamma absorbed dose rate in air (ADRA)**

It is the gamma dose at 1m above the ground level and $C_{Ra}$, $C_{Th}$ and $C_K$ are the activity concentrations of $^{226}Ra$, $^{232}Th$ and $^{40}K$ radioisotopes, respectively [25,26].

$$ADRA\left(\frac{nGy}{h}\right) = (0.427C_{Ra}) + (0.662C_{Th}) + (0.042C_K) \quad \textbf{(4)}$$

**Annual outdoor effective dose ($AED_{out}$)**

Annual outdoor effective dose ($AED_{out}$) due to γ-rays emitted from radionuclides of $^{226}Ra$, $^{232}Th$ and $^{40}K$ maintained in the selected samples was calculated from Eq. (5).

$$AED_{out}\ (mSv/year) = ADRA(nGy/h) \times 8760\ (h/year) \times 0.2 \times 0.7\ (Sv/Gy) \times \frac{10^3 mSv}{10^9 nGy} \quad \textbf{(5)}$$

Where, 0.7 Sv/Gy is a conversion coefficient for the conversion of the absorbed dose in air to the effective dose received by adults where the occupancy factor amounts 0.2 [27,28].

## RESULTS AND DISCUSSIONS

### Statistical analysis and data mining

Specific activities, their ratios to each other and related calculated gamma absorbed dose rate in air (ADRA) and annual outdoor effective dose ($AED_{out}$) were evaluated by summary statistics. Most of the publications in the literature, use average values to compare data but in the present study, the authors decided to use depiction groups like box and whisker diagrams. So, outliers, variations, mean median values etc. of the data become obvious.

As depicted in Fig.4a-c, there are two extreme values (ID: 66 for $^{226}Ra$, ID:41 for $^{40}K$ activity concentration distributions). The extent of ranges indicates natural variations that might indicate signature of the fractionation processes. The highest ranges belong to $^{40}K$ distributions. It is noticeable from this figure that activity concentrations of AG samples are higher than GD samples. Table 3 shows that the activity concentrations of the natural radionuclides of granites from other world examples are relatively higher than that of AG and GD samples.

The analysis of the ratios of radionuclide pairs indicates depletion or enrichment processes of the radioisotopes due to their magmatic process. Alterations and/or weathering processes also affect the radionuclide content of rocks [29-31]. According to Table 3, $^{226}Ra/^{40}K$, $^{232}Th/^{40}K$ and $^{226}Ra/^{232}Th$ ratios are mostly higher than that of the present study. The significant relation between $^{226}Ra$ and $^{232}Th$ may be explained by investigating the geological formation and chemical composition of the granite in addition to the close system equilibrium model is possibly applicable to study the relation between the different isotopes and the relationship between parent and its daughters such as $^{234}U/^{238}U$, $^{230}Th/^{234}U$ and $^{226}Ra/^{232}Th$, which reflect the water-rock [32-33] interaction in the environment.

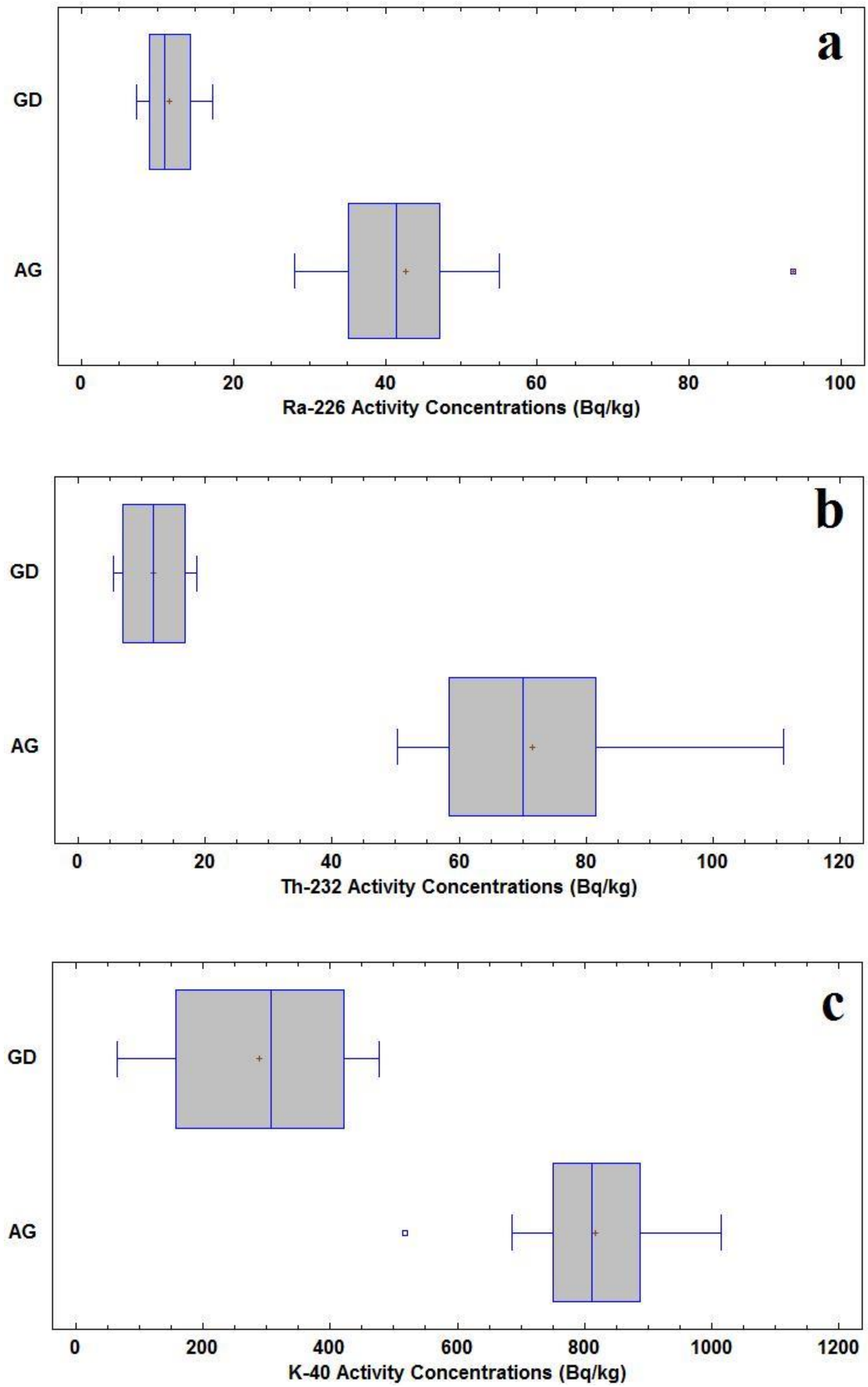


**Fig. (4):** Comparison of the a) Ra-226, b) Th-232 and c) K-40 activity concentrations of the samples in terms of granodiorite (GD) and albite granite (AG) rock types/varieties using the box and whisker plots.

**Analyzes of ADRA and AEDout indexes**

**Absorbed Gamma Dose Rate in Air (ADRA)**

According to Table 2, the dose rates of albite granite samples are higher than that of the granodiorite samples. In addition, the highest gamma contributions mostly come from $^{40}$K in granodiorites, and $^{232}$Th in albite granites (Fig.5a-b). Similar studies focused on absorbed gamma dose rate and hazard indexes from different materials such as cement, tiles, gravel, bricks and tuff have been done in the world [21,30,31,34,35]. From the radiological point of view, the results of the various absorbed radiation dose rates for the corresponding materials are all lower than the obtained results from granite in the present study. In addition, absorbed gamma dose rates of the granites from other countries all over the world (Table 3) are relatively higher than the values presented in the present study.

**Annual outdoor effective dose ($AED_{out}$)**

From data in Table 2, it reveals that the values of albite granite samples are higher than the granodiorite samples. Additionally, average values of albite granites and granodiorites for ADRA and $AED_{out}$ values are relatively higher than the minimum values of the granite samples gathered from literature (Table 3).

Comparison of the radionuclide content contributions for AED values is not determined because that index is calculated from the ADRA.

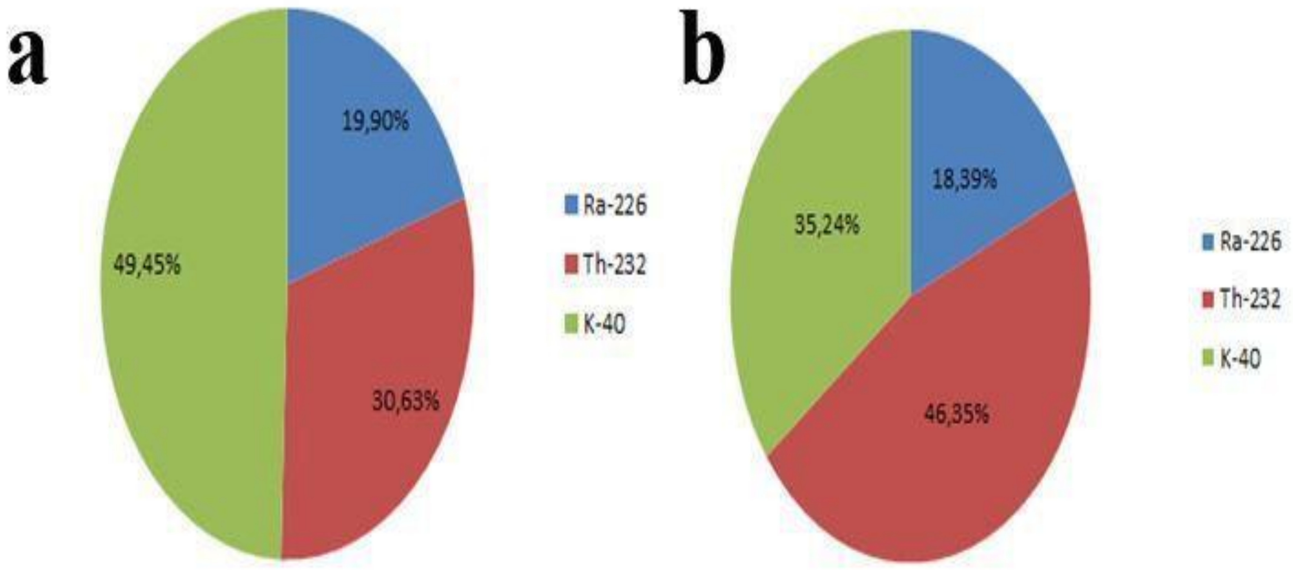


**Fig. (5a-b):** Radionuclide content contributions for absorbed gamma dose rate (ADRA) values in terms of the rock groups. **a)** ADRA values of gronadiorite (GD) samples, **b)** ADRA values of albite granite (AG) samples.

**Table (1): Specific activities of $C_{Ra-226}$, $C_{Th-232}$ and $C_{K-40}$ for the studied albite granite and granodiorite samples from Nuweibi mining area, Egyptian Nubian Shield.**

| Sample No. (ID) | Sample type | Radium activity concentration $C_{Ra-226}$ (Bq/kg) | Thorium activity concentration $C_{Th-232}$ (Bq/kg) | Potassium activity concentration $C_{K-40}$ (Bq/kg) | $^{226}Ra/^{40}K$ | $^{232}Th/^{40}K$ | $^{226}Ra/^{232}Th$ |
|---|---|---|---|---|---|---|---|
| 1 | Granodiorite | 10.7 ± 0.6 | 8.6 ± 0.5 | 65 ± 3 | 0.16 | 0.13 | 1.24 |
| 2 | Granodiorite | 17.2 ± 1.2 | 14.9 ± 1.2 | 364 ± 17 | 0.05 | 0.04 | 1.15 |
| 15 | Granodiorite | 11.2 ± 0.7 | 18.6 ± 1.0 | 477 ± 20 | 0.02 | 0.04 | 0.61 |
| 47 | Granodiorite | 7.3 ± 0.4 | 5.5 ± 0.3 | 250 ± 10 | 0.03 | 0.02 | 1.31 |
| 7 | Albite granite | 42.6 ± 2.6 | 56.9 ± 2.7 | 989 ± 41 | 0.04 | 0.06 | 0.75 |
| 8 | Albite granite | 37 ± 2.2 | 56.6 ± 2.7 | 1014 ± 42 | 0.04 | 0.06 | 0.65 |
| 9 | Albite granite | 54.9 ± 3.3 | 65.1 ± 3.1 | 856 ± 35 | 0.06 | 0.08 | 0.84 |
| 11 | Albite granite | 45.2 ± 2.7 | 58.1 ± 2.8 | 827 ± 34 | 0.05 | 0.07 | 0.78 |
| 12 | Albite granite | 40.3 ± 2.4 | 58.5 ± 2.7 | 695 ± 29 | 0,06 | 0.08 | 0.69 |
| 13 | Albite granite | 45.4 ± 2.7 | 60 ± 2.8 | 788 ± 33 | 0.06 | 0.08 | 0.76 |
| 16 | Albite granite | 28.1 ± 1.7 | 85 ± 4.0 | 685 ± 28 | 0.04 | 0.12 | 0.33 |
| 17 | Albite granite | 35.9 ± 2.2 | 57.2 ± 2.8 | 935 ± 39 | 0.04 | 0.06 | 0.63 |
| 19 | Albite granite | 43.2 ± 2.6 | 81.6 ± 3.8 | 808 ± 33 | 0.05 | 0.10 | 0.53 |
| 20 | Albite granite | 28 ± 1.7 | 68.3 ± 3.2 | 886 ± 37 | 0.03 | 0.08 | 0.41 |
| 29 | Albite granite | 32.1 ± 1.9 | 67.2 ± 3.1 | 801 ± 33 | 0.04 | 0.08 | 0.48 |
| 30 | Albite granite | 39.2 ± 2.3 | 71.3 ± 3.3 | 803 ± 33 | 0.05 | 0.09 | 0.55 |
| 31 | Albite granite | 48.5 ± 2.9 | 50.2 ± 2.4 | 729 ± 30 | 0.07 | 0.07 | 0.97 |
| 34 | Albite granite | 49 ± 2.9 | 73.1 ± 3.5 | 803 ± 33 | 0.06 | 0.09 | 0.67 |
| 36 | Albite granite | 28.3 ± 1.7 | 76.7 ± 3.6 | 751 ± 31 | 0.04 | 0.10 | 0.37 |
| 41 | Albite granite | 29.2 ± 1.7 | 72.3 ± 3.4 | 518 ± 21 | 0.06 | 0.14 | 0.40 |
| 44 | Albite granite | 35.1 ± 2.1 | 68.8 ± 3.2 | 686 ± 29 | 0.05 | 0.10 | 0.51 |
| 45 | Albite granite | 46.6 ± 2.8 | 85.7 ± 4.1 | 814 ± 34 | 0.06 | 0.11 | 0.54 |
| 46 | Albite granite | 36.1 ± 2.2 | 83.6 ± 3.9 | 823 ± 34 | 0.04 | 0.10 | 0.43 |
| 65 | Albite granite | 47.1 ± 3.5 | 80.9 ± 5.8 | 930 ± 48 | 0.05 | 0.09 | 0.58 |
| 66 | Albite granite | 93.6 ± 5.6 | 111 ± 5.2 | 930 ± 39 | 0.10 | 0.12 | 0.84 |
| 67 | Albite granite | 51.4 ± 3.1 | 86.2 ± 4.0 | 886 ± 37 | 0.06 | 0.10 | 0.60 |
| Mean | Granodiorite | 11.2 | 11.9 | 289 | 0.065 | 0.05 | 1.077 |
| | Albite granite | 42.2 | 71.5 | 811 | 0.052 | 0.09 | 0.60 |
| Standard deviation | Granodiorite | 4.2 | 5.5 | 175 | 0.064 | 0.04 | 0.31 |
| | Albite granite | 13.8 | 14.1 | 113 | 0.01 | 0.02 | 0.17 |
| Minimum | Granodiorite | 7.3 | 5.5 | 65 | 0.02 | 0.02 | 0.61 |
| | Albite granite | 28.1 | 50.2 | 518 | 0.03 | 0.06 | 0.33 |
| Maximum | Granodiorite | 17.2 | 18.6 | 477 | 0.16 | 0.13 | 1.31 |
| | Albite granite | 93.6 | 111 | 1014 | 0.03 | 0.14 | 0.97 |

**Table (2): Calculated gamma absorbed dose rates in air and annual outdoor effective doses of the studied albite granite and granodiorite samples from Nuweibi mining area, Egyptian Nubian Shield.**

| Sample No. (ID) | Sample type | ADRA ($nGyh^{-1}$) | AED (mSv/year) (outdoor) |
|---|---|---|---|
| 1 | Granodiorite | 13 | 0.02 |
| 2 | Granodiorite | 32 | 0.04 |
| 15 | Granodiorite | 36 | 0.05 |
| 47 | Granodiorite | 17 | 0.02 |
| 7 | Albite granite | 96 | 0.12 |
| 8 | Albite granite | 94 | 0.12 |
| 9 | Albite granite | 101 | 0.12 |
| 11 | Albite granite | 91 | 0.11 |
| 12 | Albite granite | 83 | 0.10 |
| 13 | Albite granite | 91 | 0.11 |
| 16 | Albite granite | 94 | 0.12 |
| 17 | Albite granite | 91 | 0.11 |
| 19 | Albite granite | 104 | 0.13 |
| 20 | Albite granite | 92 | 0.11 |
| 29 | Albite granite | 90 | 0.11 |
| 30 | Albite granite | 95 | 0.12 |
| 31 | Albite granite | 84 | 0.10 |
| 34 | Albite granite | 101 | 0.12 |
| 36 | Albite granite | 92 | 0.11 |
| 41 | Albite granite | 80 | 0.10 |
| 44 | Albite granite | 87 | 0.11 |
| 45 | Albite granite | 108 | 0.13 |
| 46 | Albite granite | 102 | 0.13 |
| 65 | Albite granite | 110 | 0.14 |
| 66 | Albite granite | 150 | 0.19 |
| 67 | Albite granite | 114 | 0.14 |
| Mean | Granodiorite | 24.50 | 0.03 |
| | Albite granite | 97.72 | 0.12 |
| Standard deviation | Granodiorite | 11.21 | 0.01 |
| | Albite granite | 14.58 | 0.01 |
| Median | Granodiorite | 24.50 | 0.03 |
| | Albite granite | 94 | 0.12 |
| Minimum | Granodiorite | 13 | 0.02 |
| | Albite granite | 80 | 0.1 |
| Maximum | Granodiorite | 36 | 0.05 |
| | Albite granite | 150 | 0.19 |

**Table 3: Average values of activity concentrations of $^{226}$Ra, $^{232}$Th, $^{40}$K, their ratios to each other and health hazard indexes (ADRA, $AED_{out}$) from different countries of the world given for granite samples**

| Country/origin/type of granites | No. of samples | $^{226}$Ra (Bq/kg) | $^{232}$Th (Bq/kg) | $^{40}$K (Bq/kg) | $^{226}$Ra /$^{40}$K | $^{232}$Th/ $^{40}$K | $^{226}$Ra/ $^{232}$Th | ADRA (nGy/h) | AED (mSv/year) (Outdoor) | References |
|---|---|---|---|---|---|---|---|---|---|---|
| Austria | 1 | 40 | 253 | 1340 | 0.02 | 0.10 | 0.15 | 231.93 | 0.28 | (36) |
| Belgium | 1 | 68 | 77 | 1129 | 0.06 | 0.06 | 0.88 | 126.39 | 0.15 | (37) |
| Brazil | 14 | 82 | 168 | 1297 | 0.02 | 0.12 | 0.48 | 196.55 | 0.24 | (37) |
| China | 8 | 95 | 152 | 1256 | 0.03 | 0.12 | 0.62 | 190.86 | 0.23 | (36) |
| Egypt/Wadi Karim | 10 | 56 | 54 | 4819 | 0.01 | 0.01 | 1.03 | 260.41 | 0.31 | (38) |
| Egypt/Um Taghir | 39 | 558 | 359 | 3918 | 0.14 | 0.09 | 1.55 | 644.27 | 0.79 | (38) |
| Egypt/Gable Gattar II | 10 | 6018 | 113 | 1140 | 5.27 | 0.09 | 53.25 | 2892.23 | 3.54 | (39) |
| Egypt/Gable El Majai | 10 | 198 | 30 | 681 | 0.29 | 0.04 | 6.6 | 138.36 | 0.16 | (40) |
| Egypt/Gable El Misikat | 9 | 1184 | 40 | 705 | 1.67 | 0.05 | 29.6 | 600.14 | 0.73 | (40) |
| Egypt/Gable El Aradiya | 10 | 126 | 25 | 480 | 0.26 | 0.05 | 5.04 | 93.67 | 0.11 | (40) |
| Egypt/Homert Waggat North | 10 | 489 | 109 | 1590 | 0.30 | 0.06 | 4.48 | 359.63 | 0.44 | (40) |
| Egypt/Homert Waggat South | 10 | 787 | 163 | 1302 | 0.60 | 0.12 | 4.82 | 518.64 | 0.63 | (40) |
| Egypt/ Nubian Shield (Granodiorite) | 4 | 11 | 12 | 289 | 0.03 | 0.05 | 1.91 | 24.50 | 0.03 | Present study |
| Egypt/ Nubian Shield (albite granite) | 22 | 43 | 72 | 811 | 0.05 | 0.09 | 0.60 | 97.72 | 0.12 | Present study |
| Egypt/South Sinai (Syenogranite) | 10 | 57 | 71 | 1173 | 0.04 | 0.06 | 0.80 | 119.42 | 0.15 | (1) |
| Egypt/South Sinai (Alkali feldspar granite) | 10 | 45 | 54 | 1500 | 0.03 | 0.03 | 0.83 | 116 | 0.14 | (1) |
| Egypt/South Sinai (Aplite dike) | 5 | 213 | 279 | 1268 | 0.16 | 0.22 | 0.76 | 324 | 0.40 | (1) |
| Egypt/Abu Dabbab (Albite granite) | 10 | 46 | 20 | 602 | 0.07 | 0.03 | 2.3 | 58.76 | 0.07 | (2) |
| Finland | 3 | 94 | 163 | 1223 | 0.07 | 0.13 | 0.57 | 195.88 | 0.24 | (36) |
| Greece | 49 | 77 | 91 | 929 | 0.08 | 0.09 | 0.84 | 130.92 | 0.16 | (41,42) |
| Holland | 1 | 162 | 490 | 1540 | 0.10 | 0.31 | 0.33 | 444.17 | 0.54 | (37) |
| India | 4 | 119 | 172 | 1082 | 0.10 | 0.15 | 0.69 | 207.13 | 0.25 | (36) |
| Italy | 4 | 64 | 91 | 1206 | 0.05 | 0.07 | 0.70 | 136.48 | 0.16 | (43) |
| Malaysia | 1 | 86 | 134 | 1019 | 0.08 | 0.13 | 0.64 | 165.62 | 0.20 | (36) |
| Portugal | 1 | 117 | 105 | 1490 | 0.07 | 0.07 | 1.11 | 181.45 | 0.22 | (36) |
| S. Africa | 1 | 92 | 153 | 1151 | 0.07 | 0.13 | 0.60 | 185.72 | 0.22 | (36) |
| Spain | 1 | 80 | 123 | 1289 | 0.06 | 0.09 | 0.65 | 167.26 | 0.20 | (36) |
| Sweeden | 2 | 107 | 110 | 1226 | 0.08 | 0.08 | 0.97 | 168.98 | 0.20 | (36) |
| Turkey/Kaymaz | 7 | 306 | 248 | 1266 | 0.24 | 0.19 | 1.23 | 348.36 | 0.42 | (44) |
| Turkey/Sivrihisar | 7 | 67 | 153 | 1058 | 0.06 | 0.14 | 0.43 | 170.32 | 0.20 | (44) |
| Pakistan/Ambela | 20 | 659 | 598 | 1203 | 0.54 | 0.49 | 1.10 | 726.51 | 0.89 | (45) |
| Minimum | | 12 | 12 | 307 | 0.01 | 0.01 | 0.15 | 24.88 | 0.03 | |
| Maximum | | 6018 | 598 | 4819 | 5.27 | 0.49 | 53.25 | 2892.23 | 3.54 | |

*With modifications from Papadopoulos et al., 2010 [42]

## CONCLUSIONS

The natural radioactivity of some granitic rocks in the Nuweibi mining area in the central Eastern Desert of Egypt has been measured for the first time in details. The activity concentrations of the granitic samples are variable due to the rock types (granodiorite and albite granite).

Faults and shear zones across Nuweibi albite granite (NAG) play the most important role in radioactivity because they act as pathways or channels for the hydrothermal solutions. Due to the mobilization of natural radionuclides aided by the hydrothermal solutions, the sheared albite granite outcrops were collected and their gamma-radioactivity levels along the strike-slip fault and shear zones (Fig.1) found mostly higher than the other granitic samples. The data are more likely to the radioactivity measurements of the neighbouring Abu Dabbab mining area. On the other hand, the highest gamma contributions of absorbed gamma dose rate mostly come from $^{40}K$ in the granodiorites and $^{232}Th$ in the albite granites. Accordingly, the Nuweibi albite granites mining area is mostly safe and there is no critical radiological risk in terms of human health.

**Acknowledgments**

The authors would like to thank Miss Gulcan Top, an independent researcher, Istanbul, Turkey for her help in statistical analysis of our radiometric data.

## REFERENCES

[1] Heikal, M.Th.S. and Top, G. (2018): Assessment of radioactivity levels and potential radiation health hazards of Madsus granites and associated dikes nearby and around Ruwisat village, South Sinai, Egypt. Journal of African Earth Sciences, volume 146, pp. 191-208.

[2] Heikal, M.Th.S., Gomaa, S.R., Abd El Monsef, M., Taha, A., Top, G., Mahmoud. K.R., El- Mansi, M.M. (2018a): Insight on Radiological Risk Assessment and its Statistical Evaluations for Abu Dabbab Albite Granite Mining area, Central Nubian Shield, Egypt. Arabian Journal of Nuclear Physics and Applications. DOI ajnsa.2018.12966. Vol.: 10.21608.

[3] Heikal, M,Th.S., Abd El Monsef, M., El Mansi, M., Gomaa, S.R. and Top, G. (2018b): Natural Radionuclides Levels and their Geochemical Characteristics of Abu Dabbab Albite Granite Mining Area, Central Nubian Shield of Egypt. Journal of Environmental Hazards.1.1,1-14.

[4] Krieger, V.R (1981): Radioactivity of construction materials, Betonwork Fertigteil Technol. 47 468.

[5] Beretka, J., Matthew, P.J. (1985): Natural radioactivity of Australian building materials, industrial wastes and by-products. Health Phys. 48, 87. doi:10.1097/00004032-198501000-00007

[6] El-Arabi A.M., (2007): Ra, Th, K concentrations in igneous rocks from Eastern Desert, Egypt and its radiological implications. Radiat. Meas. 42, 94-100.

[7] El-Shershaby A., (2002): Study of radioactivity levels in granite of Gable-Gattar II in the north eastern desert of Egypt. Appl. Radiat. Isot. 57, 131-135.

[8] Heikal, M.Th.S., El Dousky, B.T., Ghoneim.M.F. and Sherif,M.I. (2013): Natural Radioactivity in basement rocks and stream sediments,Sharm El Sheikh area,South Sinai,Egypt: Radiometric levels and their significant contributions. AJGS. ) 6:3229–3239. DOI: 10.1007/s12517-012-0622-6

[9] Gafar, I. (2014) Geophysical Mapping, Geochemical Evidence and Mineralogy for Nuweibi Rare Metal Albite Granite, Eastern Desert, Egypt. Open Journal of Geology, 2014, 4, 108-136.

[10] Helba, H., Trumbull, R. B., Morteani, G., Khalil, S. O., and Arslan, A. (1997): Geochemical and petrographic studies of Ta mineralization in the Nuweibi albite granite complex, Eastern Desert, Egypt. Miner. Depos. 32:164–179.

[11] Emam, A., Zoheir, B., Radwan, A.M., Lehmann, B., Zhang, R., Fawzy,S., Nolte, N. (2018): Petrogenesis and evolution of the Nuweibi rare-metal granite, Central Eastern Desert, Egypt. Arabian Journal of Geosciences 11:736

[12] Azer, M.K., Abd el fadil, K. M. and Ramadan, A.A. (2019): Geochemistry and Petrogenesis of Late Ediacaran Rare-Metal Albite Granite of the Nubian Shield: Case Study of Nuweibi Intrusion, Eastern Desert, Egypt. The Journal of Geology, volume 127, DOI: 10.1086/705328.

[13] Canberra Industries, USA, Genie™ 2000 Spectroscopy Software, Operations V3.1 in 1 Apr 2003.

[14] Chieco, N.A., Bogeen, D.C., Knutson,E.O. (1990): Environmental Measurements Laboratory (EML),

the procedures manual, HASL-300, ED.27-Vol edition issued November 1990.

[15] Povinec, P. P. et al., (2002): Journal of Radioanalytical and Nuclear Chemistry, Vol. 251, No. 3, 369–374, Certified reference material for radionuclides in seawater (Irish Sea Water).

[16] Pszonicki, L., A.N. Hanna, A.N., and Suschny, O. (1984): Report on Intercomparison IAEA/SOIL-6, International Atomic Energy Agency, IAEA/RL/111.

[17] Torres Astorga, R., Rizzotto, M.G., and Velasco, H. (2019): Improving the efciency in the detection of gamma activities in environmental soil samples: influence of the granulometry and soil density. Journal of Radioanalytical and Nuclear Chemistry Vol. 321:805–814.

[18] Penabei, D. Bongue, P. Maleka, T. Dlamini, Saïdou, C.J. Guembou Shouop, Y.I. Halawlaw, A. Ngwa Ebongue and M.G. Kwato Njock (2018): assessment of natural radioactivity levels and the associated radiological hazards in some building materials from Mayo-Kebbi , region, Chad, J. Radioprotection, 0-30.

[19] Yücel H., Karadeniz H., Çetiner M. A., Demirel H., Turhan S. (2003): Measurement of absolute intensity of 1001 keV gamma-ray of 234mPa Journal of Radioanalytical and Nuclear Chemistry, Vol. 258, No. 2, 445–447.

[20] Aku, M.O. and Yusuf, U. (2015): Radiological evaluation of building materials used in Malumfashi, Katsina State, using gamma-ray spectroscopy, Analysis, Bajopas Volume 8.

[21] Trevisi, R., Risica, S., D'Alessandro, M., Paradiso, D., Nuccetelli, C. (2012): Natural radioactivity in building materials in the European Union a database and an estimate of radiological significance. J. Environ. Radioact. 105, 11e20. Doi: 10.1016/j.jenvrad.2011.10.001.

[22] Stephen Kaiser, European Commission, Radiation protection 112, Radiological Protection Principles concerning the Natural Radioactivity of Building Materials 1999.

[23] Lépy, M C., Pearce, A., and Sima, O. (2015): Uncertainties in gamma-ray spectrometry, journal of Metrologia 52, S123–S145.

[24] Guembou, S. C. J., Samafou, P., Moyo M. N., Gregoire, C., Eric J. N. M., Alexandre, N. E., Motapon, O., and Strivay, D. (2017): Precision measurement of radioactivity in gamma-rays spectrometry using two HPGe detectors comparison techniques: Application to the soil measurement. Journal of MethodsX V.4, 42–54.

[25] Beck, H.L. (1980): Exposure Rate Conversion Factors for Radionuclides Deposited on the Ground. Report no.EML-378.NY. US, Department of Energy.

[26] International Commission on Radiological Protection (1991): Recommendations of the International Commission on Radiological Protection, Annals of the ICRP, 21, 1-3.–473.

[27] UNSCEAR (1988): United Nations Scientific Committee on the Effects of Atomic Radiation. Sources and Biological Effects of Ionizing Radiation, United Nations, New York.

[28] UNSCEAR (2000): Source and Effects of Ionizing Radiation. Report to General Assembly, with Scientific Annexes. United Nations Scientific Committee on the Effects of Atomic Radiation. United Nations, New York, 265-273.

[29] Chiozzi, P., Pasquale, V., Verdoya, M. (2002): Naturally occurring radioactivity at the Alps-Apennines transition. Radiat. Meas. 35, 147-154.

[30] Top, G., Örgün, Y., Karahan, G., Horvath, M., and Kampfl, G. (2020): Effects of Local Building Materials on Indoor Gamma Doses and Related Radiological Health Risks, Ayvacık, Çanakkale/Turkey. Radiat. Prot. Dosimetry, 190(1), 108–117. doi:10.1093/rpd/ncaa086.

[31] Top, G., Örgün, Y., Karahan, G., Özcan,O., Horvat, M. and Kampfl, G. (2019): At high back-ground radiation areas the relatıonship between insitu indoor gamma dose rates and building materials: a case study from Arıklı village (Ayvacık/Çanakkale/Turkey). Radiat. Prot. Dosimetry, ncz282. doi:10.1093/rpd/ncz282.

[32] Giggenbach W.F. (1984): Mass transfer in hydrothermal alteration systems—A conceptual approach. Geochimica et Cosmochimica Acta 48: 2693-2711

[33] Zuddas P, Seimbille F, Michard G. (1995): Granite-fluid interaction at near equilibrium conditions: Experimental and theoretical constrains from Sr contents and isotopic ratios. Chemical Geology 121: 145-154).

[34] Ngachin M, Garavaglis M, Giovani C, Kwato Njock MG, Nourreine A. (2007): Assessment of natural radioactivity and associated radiation hazards in some Cameroonian building materials, Radiat. Meas. 42: 61–67.

[35] Amrani D, Tahtat M. (2001): Natural radioactivity in Algerian building materials, Appl. Radiat. Isot. 54: 687–689.

[36] Chen C.J., Lin Y.M. (1996): Assessment of building materials for compliance with regulations of ROC. Environment International 22, 221-226.

[37] Tzortzis M., Tsertos H., Christofides S., Christodoulides G. (2003): Gamma measurements and dose rates in commercially used tiling rocks (granites). Journal of Environmental Radioactivity 70, 223-235.

[38] El-Arabi A.M. (2007): Ra, Th, K concentrations in igneous rocks from eastern desert Egypt and its radiological implications. Radiat. Meas. 42, 94-100.

[39] El-Shershaby A., (2002): Study of radioactivity levels in granite of Gable-Gattar II in the north eastern desert of Egypt. Appl. Radiat. Isot. 57, 131-135.

[40] Arafa W. (2004): Specific activity and hazards of granite samples collected from the eastern desert of Egypt. J. Environ. Radioactivity. 75, 315-327.

[41] Karavasili E., Christofides G., Papastefanou C., Koroneos A. and Stoulos S. (2005): Mineralogy, Petrography and Radioactivity of Greek Granites. Proceedings of the 2nd Congress of the Committee of the Economic Geology, Mineralogy & Geochemistry of the Geological Society of Greece, Thessaloniki, 123-132.

[42] Papadopoulos A., Christofides G., Papastefanou C., Koroneos A.,and Stoulos S. (2010): Radioactivity of granitic rocks from northern Greece. Bulletin of the Geological Society of Greece, 2010 Proceedings of the 12th International Congress Patras.

[43] Menager M.T., Heath M.J., Ivanovich M., Montjotin C., Barillon C.R., Camp J. and Hasler S.E. (1993): Migration of uranium from uranium-mineralised fractures into rock matrix in granite: implications for radionuclide transport around a radioactive waste repository. Radfiochem. Acta 66/67 47-83.

[44] Örgün Y. and Altınsoy N. (2005): Natural radioactivity levels in granitic plutons and groundwaters in southeast part of Eskisehir, Turkey. Appl. Radiat. Isot. 63, 267-275.

[45] Asghar M., Tufail M., Javied S., Abid A. and Waqas M. (2008): Radiological implications of granite of northern Pakistan. J. Radio. Protection 28, 387-399.